Surface Energy Balance and Turbulence Characteristics Observed at the SHEBA Ice Camp During FIRE III

Peter G. Duynkerke[1] and Stephan R. de Roode[2]

[1]IMAU, Utrecht University, Princetonplein 5, 3584 CC Utrecht, The Netherlands

Email: P.G.Duynkerke@phys.uu.nl

[2]Stephan de Roode, University of Washington, Department of Atmospheric Sciences,

Box 351640, Seattle, WA 98195-1640, U.S.A.

email: roode@atmos.washington.edu

13 December 1999, submitted to Journal of Geophysical Research

for the FIRE.ACE special issue

Accepted September 2000

Abstract

The Institute for Marine and Atmospheric Research Utrecht (IMAU) participated in the FIRE III (First ISCCP Regional Experiment, ISCCP International Satellite Cloud Climatology Project) experiment in May 1998. In this paper we describe surface layer measurements performed on the sea ice at the SHEBA (Surface Heat and Energy Balance of the Arctic ocean) camp and compare these with measurements collected above a grass-covered surface in Cabauw, the Netherlands. The observations consist of both high-frequency turbulence measurements and mean-profile measurements of wind, temperature and humidity. In addition, we measured the upward and downward components of both the longwave and shortwave radiation, and the snow and ice temperatures in the upper 40 cm. The observations give a detailed picture of all components of the energy balance of the Arctic sea-ice surface.

The turbulence measurements are used to study the surface layer scaling of the turbulence variables in the stable boundary layer. More specifically, we showed that the integral length scale of the vertical velocity fluctuations serves as the relevant turbulence length scale. The monthly-averaged energy balance of the Arctic sea-ice was dominated by radiative fluxes, whereas, the sensible and latent heat flux and the energy flux into the surface were rather small. A detailed inspection of the diurnal variations in the turbulent fluxes however indicates that although the monthly-averaged values are small, the hourly-averaged values for these fluxes are significant in the surface energy balance.

1. INTRODUCTION

Continuous atmospheric surface-layer measurements made in the Arctic region are rather scarce. The harsh climatological circumstances, together with a floating ice surface that can suddenly crack or gradually melt, hinder the maintenance of permanent weather stations. Untersteiner (1961) presented observations of the heat budget of arctic sea ice during a seasonal cycle from a drifting station. The Arctic region is of primary climatological importance. For example, many general circulation models (GCM) predict global warming which is most significant near the North and South Pole. Usually the accuracy of these models is assessed by performing a GCM simulation and comparing the results with routine observational data and climatology. If the GCM is found to simulate the past climate accurately then this adds some weight to predictions of the future climate. Verifying the model's performance in the Arctic region however, is rendered difficult by the lack of a long-term sequence of field observations.

To gain a better understanding about the Arctic climate a team of scientists collected a comprehensive set of atmospheric measurements in the Arctic region during 1997 and 1998 as part of the SHEBA and FIRE III (Surface Heat and Energy Balance of the Arctic Ocean and First ISCCP Regional Experiment, respectively) field experiments. In the SHEBA experiment the emphasis was on surface processes. FIRE III was concerned primarily with Arctic clouds. The SHEBA observations were made on the sea ice, whereas the FIRE III program included aircraft and satellite observations. Usually the aircraft flew in the vicinity

of the SHEBA ice camp. The measurements can be used to compare in-situ data with modeling results and to obtain more detailed knowledge about the physical processes in the atmosphere such as cloud microphysics, radiation and boundary-layer turbulence.

The research foci of FIRE III and SHEBA clearly reflect the most important, and possibly the most uncertain factors that play a key role in the Arctic climate: clouds and surface fluxes. Clouds significantly modify the incoming solar radiation by reflection and absorption, and at the same time they increase the downward component of the longwave radiation. The cloud optical-properties are determined mainly by the cloud-droplet distribution and the vertically integrated cloud-water content. Errors in these quantities and uncertainties in the surface fluxes give rise to an incorrect surface energy balance and can seriously degrade the performance of other aspects of GCM simulation. A comparison between the ECMWF forecast model and SHEBA observations is reported in Beesley et al. (2000) and Bretherton et al. (2000). The cloud fields generated by the ECMWF model were in fairly good agreement with the observations. However, modeled surface fluxes and temperatures could differ significantly from the results of observations; this could have been due to the use of a single-slab ice-layer model.

Utrecht University participated in the FIRE III experiment during May 1998. The SHEBA ice camp (76^{o}N, 166^{o}W) was used as a base for operating a tethered balloon. The balloon was equipped with a radiometer to measure actinic flux (the radiance integrated over 4π steradian) of the visible light in Arctic clouds (Roode et al., 2000). Another part of the

Utrecht University measurement program involved surface-layer measurements. High-frequency measurements of the three components of the wind velocity and of thermodynamic variables in the surface layer were collected. In addition, longwave and shortwave radiation measurements and observations of wind velocity and direction, temperature and humidity were made from a 10 m mast. Since the temperatures in the upper layer of the ice sheet were measured too, we could obtain a detailed picture of the surface energy balance of the Arctic sea ice. In addition an instrument (PVM-100A) was installed on the sea ice to measure the liquid water content and cloud droplet effective radius in fog when the cloud base was near the ground surface.

In the Arctic the boundary layer is often stably stratified. The turbulence structure of the stable boundary layer (SBL) is rather complicated. In a stable vertical temperature stratification vertical disturbances are damped such that the turbulence intensity in an SBL is rather weak and may be intermittent (Derbyshire, 1990; Mahrt, 1998; Andreas, 1987). Due to the lack of a definite theory, the general method used to describe a turbulent flow involves the use of similarity relationships. In general, similarity theory involves selecting variables which are relevant to the problem and organizing these into non-dimensional groups (Garratt, 1992; Högström 1988, 1996; Stull, 1988). For example, Caughey et al. (1979), Mahrt et al. (1979) and Yamada (1979) presented turbulence variables in an SBL in terms of the surface-layer momentum (u_*^2) and potential temperature ($\overline{w'\theta'}$) flux, as a function of z/H, where H is the boundary-layer height. Nieuwstadt (1984) argued that the boundary-layer height H

cannot be taken as a representative length scale because in a stable temperature stratification turbulent eddies do not extend across the whole boundary layer. On the basis of theoretical considerations (Wyngaard, 1975; Brost and Wyngaard, 1978), and supported by observations, Nieuwstadt advocated the so-called z-less scaling hypothesis. According to this hypothesis, the dimensionless variables, which are measured at the same height, can be expressed uniquely as a function of the stability parameter z/Λ, where Λ is the local Monin-Obukhov length. In section 3.1 it is argued that instead of z/Λ one can also use the gradient Richardson number as a stability parameter. In many general circulation models and weather models the gradient Richardson number is typically used to parametrize the effect of the stable stratification on the fluxes. In section 3.3 the parametrizations used in the European Centre for Medium-Range Weather Forecasts (ECMWF) model will be compared with the observations discussed in this paper.

In this paper, we investigate whether the integral length scale can serve as the relevant turbulence length scale in the surface layer of the SBL. One can argue that the integral length scale is a natural candidate to serve as a relevant length scale since it represents the size of the energetically most dominant eddies. Furthermore, we will assess the effect of the filter length scale on the magnitude of several turbulence variables. This is explored by computing the ogive, which is the integral of co-spectra between a frequency f and the Nyquist frequency (Davis et al., 1996). After this analysis the monthly-averaged energy balance of the Arctic sea ice during May 1998 will be presented. In addition, we will give some

examples of diurnal variations in the radiative and turbulent fluxes, and variations in temperatures in the upper layer of the ice sheet. These measurements will illustrate that the ice sheet responds on a short time scale to processes such as turbulent and radiative fluxes at the surface.

2 INSTRUMENT and SITE DESCRIPTION

2.1 Instrumentation

High-frequency temperature and wind velocity measurements were performed by a CSAT-3 sonic anemometer from Campbell Scientific (Campbell Scientific, 1996). High-frequency humidity fluctuations were measured with a Lyman-Alpha hygrometer made by Mierij Meteo (Mierij Meteo, 1997). The sonic anemometer and Lyman-Alpha hygrometer both sampled at a frequency of 20 Hz. The measurement path length of the sonic is 10.0 cm in the vertical and 5.8 cm in the horizontal. From the data we were able to calculate the turbulent fluxes of heat, moisture and momentum.

The lowest part of the ABL was observed by instruments fixed to a 10 meter high profile mast. Wind speed, temperature and humidity were measured at heights of about 1, 2, 3, 6 and 9 meters above the surface. Radiation (Eppley precision pyrgeometers and CM14 Kipp pyranometers) at 2 meters and wind direction at 3 and 9 meters were observed every 12 seconds. Two-minute averages of these quantities were stored in a data logger. Humidity and temperature were sampled once every two minutes. Temperature and relative humidity were

measured by ventilated Vaisala temperature and humidity probes, with an estimated absolute accuracy of 0.3 ˚C and 3%, respectively. By an intercalibration at one height the relative error between five temperature sensors was found to be less than 0.1 ºC. The wind speed at the five levels was measured using cup anemometers from Campbell Vector. When these instruments were calibrated in the KNMI wind tunnel in De Bilt, the Netherlands, they were found to be accurate within 0.2 ms^{-1}. The two wind vanes used to measure wind direction were also manufactured by Campbell. The output of these instruments was only used in qualitative analysis to check the wind turning with height.

The turbulence measurements together with measurements made with instruments fixed to the profile mast are used to analyze the turbulence characteristics in the surface layer. In this paper we concentrate on observations obtained at the SHEBA ice camp during FIRE III (section 2.2) but we also use observations made with the same instrumentation at Cabauw the Netherlands (section 2.3).

2.2 SHEBA

The Institute for Marine and Atmospheric Research Utrecht (IMAU) participated in the FIRE III experiment in May 1998. On the sea ice at the SHEBA camp (about 76^{o}N, 166^{o}W) we performed surface-based measurements of longwave, shortwave and UV-B components (incoming and outgoing) of the radiative flux. The liquid water content and effective radius of the droplets were measured with a Gerber PVM-100A at about 2.2 m

above the surface. The sonic anemometer and Lyman-Alpha hygrometer were placed at a height of 2.7 m above the snow surface. The arms were pointed in a direction about 340^{o} from true North. Wind speed, temperature and humidity were measured at heights of about 1.1, 2.2, 3.2, 5.2 and 8.9 meters above the surface. In addition, snow and ice temperatures were measured at 5 depths: 5, 10, 20, 30 and 40 cm. The total thickness of the sea ice in May 1998 was about 2 m. At the SHEBA site the upper 15 cm of the surface consists of compact snow. Below 15 cm depth the surface is entirely made up of ice. Because of the snow layer on top the albedo of the surface is high: 0.82. The surface roughness length for momentum is about 0.5 mm.

A vertical profile of the atmosphere was obtained by instruments attached to a helium-filled balloon; these provided temperature, wind velocity and direction, relative humidity and (visible light) actinic flux. The results of the actinic flux measurements are described in the paper by Roode et al. (2000).

2.3 Cabauw

After the SHEBA/FIRE III experiment the same equipment was installed for two months near the Cabauw tower in the Netherlands. High-frequency temperature and wind measurements were performed with the sonic anemometer from October to November 1998: Julian Day 293 to 317. The height of the sonic was 3.45 m. Wind speed, temperature and humidity were measured at heights of about 1.2, 2.2, 3.2, 5.6 and 9.2 meters above the surface.

The instruments were situated about 200 m north of the Cabauw tower on the so-called "micro-meteorological experimental site" (Van Ulden and Wieringa, 1996; Monna and van der Vliet, 1987). The grass is kept at a height of several centimeters and the local roughness length for momentum is about 8 mm. We used only data for hours during which the wind blew from the sector 160º to 300º because in that direction there is a reasonably homogeneous fetch.

3. TURBULENCE CHARACTERISTICS

3.1 Theory of Local Scaling and Parameterization of Fluxes

The turbulent structure of the atmospheric boundary layer can be studied in more detail by inspection of the turbulent kinetic energy budget. In horizontally homogeneous conditions the turbulent kinetic energy (E) equation (Garratt, 1992) reads

$$\frac{\partial E}{\partial t} = \underbrace{-\overline{u'w'}\frac{\partial \bar{u}}{\partial z} - \overline{v'w'}\frac{\partial \bar{v}}{\partial z}}_{S} + \underbrace{g\frac{\overline{w'\theta_v'}}{\theta_0}}_{B} \underbrace{- \bar{w}\frac{\partial E}{\partial z} - \frac{\partial}{\partial z}\left(\overline{w'E'} + \frac{\overline{w'p'}}{\rho_0}\right)}_{T} \underbrace{- \varepsilon}_{D}, \qquad (3.1)$$

in which (u, v, w) are the winds in the (x, y, z) direction, g the acceleration due to gravity, θ_v the virtual potential temperature, p pressure and ε the viscous dissipation of turbulent kinetic energy. θ_o and ρ_o are constants and are prescribed as 288 K and 1.2 kg m^{-3}, respectively. The Reynolds average is denoted by an over-bar and the turbulent fluctuations by a prime. In (3.1)

the terms on the right-hand side are the shear production (S), buoyancy production (B), mean vertical advection (subsidence), turbulent transport (T) and viscous dissipation (D). Note that in the buoyancy production term the density fluctuations have been replaced by virtual potential temperature fluctuations.

For steady state conditions and when we can neglect the turbulent transport and subsidence terms the turbulent kinetic energy equation (3.1) reduces to:

$$0 = -\overline{u'w'}\frac{\partial \bar{u}}{\partial z} \quad -\overline{v'w'}\frac{\partial \bar{v}}{\partial z} + \frac{g}{\theta_0}\overline{w'\theta_v'} \quad - \varepsilon \, . \tag{3.2}$$

Equation (3.2) indicates that the kinetic energy budget is completely determined by local parameters. In that case we can express the fluxes in terms of their local gradients using the turbulent exchange coefficient K_m :

$$\left(\overline{u'w'} \, , \, \overline{v'w'}\right) = - K_m\left(\partial\bar{u}/\partial z \, , \, \partial\bar{v}/\partial z\right) . \tag{3.3}$$

With (3.3) and the definition

$$u_*^2 \equiv \left(\overline{u'w'}^{\,2} + \overline{v'w'}^{\,2}\right)^{1/2}$$

the shear production (S) in (3.2) can be written as

$$S = u_*^2\left((\partial \bar{u}/\partial z)^2 + (\partial \bar{v}/\partial z)^2\right)^{1/2}$$

Using this relation and multiplying (3.2) by $\kappa z/u_*^3$ we obtain:

$$0 = \phi_m + z/\Lambda - \phi_\varepsilon ,$$
$$\text{with: } \phi_m = \frac{\kappa z}{u_*}\left((\partial\bar{u}/\partial z)^2 + (\partial\bar{v}/\partial z)^2\right)^{1/2} , \Lambda = \frac{-u_*^3}{\kappa\, g/\theta_0\, \overline{w'\theta_v'}} , \phi_\varepsilon = \frac{\kappa z}{u_*^3}\varepsilon . \qquad (3.4)$$

The Von Kármán constant is taken as $\kappa = 0.4$. According to equation (3.4), the local dimensionless wind shear and dissipation depend only upon the stability parameter z/Λ. This is the most general form of local scaling and is used in the stable boundary layer and the surface layer. Note that for all fluxes the local values should be used and not the surface values.

Usually the ϕ_m and $\phi_h = -\kappa z u_*(\partial\overline{\theta_v}/\partial z)/\overline{w'\theta_v'}$ are expressed as a function of z/Λ. From the equations above it is possible to write the gradient (Ri_g) and flux (Ri_f) Richardson numbers in terms of z/Λ:

$$Ri_g \equiv \frac{\frac{g}{\theta_o}\frac{\partial\overline{\theta_v}}{\partial z}}{\left(\frac{\partial\bar{u}}{\partial z}\right)^2 + \left(\frac{\partial\bar{v}}{\partial z}\right)^2} = z/\Lambda\frac{\phi_h}{\phi_m^2} \quad \text{and} \quad Ri_f \equiv \frac{\frac{g}{\theta_0}\overline{w'\theta_v'}}{\overline{u'w'}\frac{\partial\bar{u}}{\partial z} + \overline{v'w'}\frac{\partial\bar{v}}{\partial z}} = z/\Lambda\frac{1}{\phi_m} . \qquad (3.5)$$

Given ϕ_m and ϕ_h as a function of z/Λ makes that from the expression (3.5) the gradient Richardson number (Ri_g) can be calculated as a function of z/Λ; as a result one can also

calculate ϕ_m and ϕ_h as a function of Ri_g: ϕ_m (Ri_g) and ϕ_h (Ri_g). In addition one can obtain an expression for the exchange coefficients for momentum (m) and heat (h):

$$K_m = f_m (\kappa z)^2 \left|\frac{\partial \mathbf{v}}{\partial z}\right| \quad \text{and} \quad K_h = f_h (\kappa z)^2 \left|\frac{\partial \mathbf{v}}{\partial z}\right| , \qquad (3.6)$$

in which f_m and f_h are defined as: $f_m = \phi_m^{-2}$ and $f_h = \phi_m^{-1} \phi_h^{-1}$. The expressions for f_m and f_h are thus a function of the stability parameter z/Λ, or by (3.5) a function of the gradient Richardson number Ri_g. In large-scale models the expressions for f_m and f_h are generally empirically chosen. For instance in the ECMWF forecast model the f_m and f_h functions are specified differently for the surface layer (between surface and first model level above the surface) and for the remaining part of the stable boundary layer (Beljaars and Viterbo, 1998). In section 3.3 we will discuss the impact of these empirical expressions.

3.2 Data treatment

The measurement frequency was 20 Hz and the raw data were stored in one-hour files. The observed wind is rotated such that the new wind components (u, v, w) are defined in the (x, y, z) direction for which we have: $\overline{v} = \overline{w} = 0$. Notice that according to surface layer theory this implies that $\overline{v'w'} = 0$. However, in practice this equality never holds and therefore we only accept data for which we have $|\overline{v'w'} / \overline{u'w'}| < 0.4$.

An FFT was performed on these data and from these the co-spectra ($Co_{\alpha\beta}(f)$) were calculated as a function of frequency (Garratt, 1992). The co-spectrum gives the contribution to the co-variance ($\overline{\alpha'\beta'}$) in the frequency range f to f + df. The influence of a cut-off filter length scale on the magnitude of various co-variances was determined by computing ogives. The ogive, $Og_{\alpha\beta}(f)$, is the integral of co-spectra between a frequency f and the Nyquist frequency. From the co-spectrum we calculate the ogives ($Og_{\alpha\beta}(f)$) defined as (Oncley et al., 1996):

$$Og_{\alpha\beta}(f) = \int_f^{\infty} Co_{\alpha\beta}(f)\, df \quad . \qquad (3.7)$$

The ogive thus equals the contribution to the co-variance (variance for energy spectrum) made by all frequency components above frequency f. In order to obtain a properly defined Reynolds-average co-variance the ogive should converge (Davis et al., 1996). Ogives are very suitable tools for this kind of analysis, since the graphical representation of the ogive clearly shows to what extent the large (meso-)scales contribute to the co-variance. In an ideal situation one would expect to find the minimum in the spectral energy within a frequency range near the spectral gap that is supposed to separate the small-scale turbulent fluctuations from the larger meso-scale motions. If the frequency f is in the spectral gap range, the ogive of the co-spectrum would produce a constant value. As an example the ogives for $\overline{u'u'}$, $\overline{v'v'}$, $\overline{w'w'}$, $\overline{u'w'}$ and $\overline{v'w'}$ are shown in Figure 1 for 1100 to 1200 UTC 1 May 1998. All ogives,

except those for $\overline{u'u'}$ and $\overline{v'v'}$, clearly converge at low frequencies. Clearly a statistically significant value for the momentum fluxes and $\overline{w'w'}$ can be calculated but the value found for the horizontal velocity variances has no statistical significance. Figure 2 shows the corresponding ogives for the temperature and humidity variances and fluxes. Here too the fluxes converge nicely, whereas the variances do not give a unique Reynolds-averaged value.

3.3 Local scaling

Since the spectra of the horizontal velocity, temperature and humidity do not exhibit a spectral peak the variances ($\sigma_\psi^2 \equiv \overline{\psi'\psi'}$) of these variables do not converge to a unique Reynolds-averaged value. Therefore in order to obtain a proper surface layer scaling we use only the filtered variances up to f = 0.01 Hz: Og(0.01). The standard deviations of the vertical velocity fluctuations normalized with the friction velocity are shown in Figure 3. The average values of the normalized standard deviations of the u, v and w fluctuations are given in Table 1 for both the filtered and unfiltered data. As a result of filtering, the values of σ_w and u_* are reduced by about 2 and 8 %, respectively. Table 1 shows that σ_w/u_* is hardly influenced by the filtering and that σ_u/u_* and σ_v/u_* are significantly reduced by the filtering. This can also be seen in the ogives (Figure 1) because the ogives for u and v do not converge as clearly as the ogives for the vertical wind components and momentum fluxes. Moreover, the scatter in the normalized standard deviations of the horizontal velocity components (not

shown) is very much reduced by the filtering. King (1990) drew attention to the fact that σ_u/u_* and σ_v/u_* have clearly defined lower bounds, with values of 2.2 and 1.5, respectively. His data do not show any dependence on z/Λ. King (1990) found that σ_w/u_* was also independent of z/Λ and that the values were scattered around a mean value of 1.42. Nieuwstadt also examined σ_w/u_* as a function of z/Λ and came to the conclusion that it was independent of stability with a mean value of 1.4. As shown in Table 1 we obtain the values of 2.31, 1.92 and 1.35 for the mean values of σ_u/u_*, σ_v/u_* and σ_w/u_*, respectively. These values agree reasonably well with the results obtained by King (1990) and Nieuwstadt (1984).

Furthermore we calculated the non-dimensional gradient of wind $\phi_m = \kappa z(\partial \bar{u}/\partial z)/u_*$ from the vertical gradient of the wind profile and the friction velocity. These results are plotted in Figure 4a as a function of z/Λ, where Λ is the local Monin-Obukhov length. The boundary layers observed during SHEBA were not very stable, therefore we have only eleven points with $z/\Lambda > 0.2$. For stable conditions the results can be approximated with about $\phi_m = 1 + 4\ z/\Lambda$ as was found in Cabauw by Duynkerke (1999) and Larsson (1997). The observed stability functions f_m and f_h in the turbulence exchange coefficient for momentum and heat (3.6) are given in Figure 4b and c as a function of the gradient Richardson number. The corresponding curve for the function in Figure 4a ($\phi_{m,h} = 1 + 4\ z/\Lambda$) is shown as a solid line: $f_{m,\,h} = (1 - 4\ Ri_g)^2$. Moreover, the stability functions used in the ECMWF model (Beljaars and Viterbo, 1998) in the surface layer and in the remaining part of the stable boundary layer are

given as long- and short-dashed lines, respectively. It is clear that in the ECMWF formulation for the stable boundary layer the values for f_m and f_h are too large compared with the observations. Given the wind and potential temperature gradients, this will lead to momentum and heat fluxes which are too large compared with observed values (see also Bretherton et al., 2000; Pinto et al., 1999).

3.4 Integral length scale

Up till now experiments have focused mainly on determining characteristic velocity scales in the stable boundary layer (SBL) and surface layer. A clear example is the local scaling introduced by Nieuwstadt (1984) for the stable boundary layer. He showed that the surface layer scaling can be extended throughout the SBL if the local friction velocity and local Monin-Obukhov length are used. The flux-profile functions ϕ_m and ϕ_h constitute the only exception: they are always defined as having the height z above the surface in their definition. Here we will investigate whether we can replace z by a more relevant length scale: the integral length scale. Future studies will have to discover whether this can be extended to more complex SBLs: katabatic flows (Van der Avoird and Duynkerke, 1999), an SBL with low-level wind maximum (Smedman et al., 1995), etc.

One way to estimate the characteristic length scales of the energy-containing eddies is to use the integral length scale Λ_ψ for variable ψ. The inverse integral length scale, Λ_ψ^{-1}, corresponds roughly to the maximum of the energy spectra, which makes it a good indicator

of the size of the eddies that dominate the turbulence spectrum. The integral length scale of a variable ψ is defined as (Kaimal and Finnigan, 1994):

$$\Lambda_\psi = \int_0^\infty \rho_\psi(\xi)\, d\xi = \int_0^\infty \frac{\overline{\psi(x)\,\psi(x+\xi)}}{\sigma_\psi^2} d\xi = \bar{u} \int_0^\infty \frac{\overline{\psi(t)\,\psi(t+\tau)}}{\sigma_\psi^2} d\tau = \bar{u}\,\tau_\psi \qquad (3.8)$$

where $\rho_\psi(\xi)$ is the auto-correlation function as defined above, and ξ the space lag with respect to the x-direction. With Taylor's hypothesis Λ_ψ is derived from a time series as: $\Lambda_\psi = \tau_\psi\ \bar{u}$. The integral time scale (τ_ψ) is a rough measure of the time interval over which $\psi(t)$ is correlated with itself. Figure 5 shows an example (for 1000 to 1100 UTC 1 May 1998) of the auto-correlation function $\rho_w(\xi)$ and its integral as a function of the space lag ξ. It is shown that the integral of the auto-correlation converges nicely to the value of the integral length scale Λ_w.

We anticipate that the integral length scale will be a more relevant scaling parameter than z because it is related to the turbulent motions; z is simply the height above the ground and the integral length scale describes scales of the most energetic eddies. This seems to be in agreement with the idea of local scaling in the sense that we may now be able to find a universal function for the non-dimensional gradients at different measuring sites and for more complex boundary layers. Since it is hard to prove the existence of unique functions for ϕ_m and ϕ_h we would like to suggest changing the length scale z in $\phi_{m,h}$ from z to Λ_w:

$$\phi'_m = \frac{\kappa \Lambda_w}{u_*} \frac{\partial \bar{u}}{\partial z} \qquad (3.9)$$

where Λ_w is the integral length scale of the vertical velocity. In Figure 6 we have plotted Λ_w/z as a function of the stability parameter z/Λ. It turns out that on the stable side it can be reasonably approximated by:

$$\frac{\Lambda_w}{z} = \frac{1}{1 + 4\, z/\Lambda} \qquad (3.10)$$

which implies that ϕ'_m in (3.3) is almost independent of stability z/Λ (Figure 7) and thus that scaling of the wind gradient with the integral length scale Λ_w works reasonably well. Kaimal (1973) also investigated the behavior of the integral length scale as a function of stability, but he used the gradient Richardson number instead of z/Λ. He found that under near-neutral conditions the integral length scale of the vertical velocity divided by the measuring height yielded a value of about 1.6, 0.55 and 0.3 for Λ_u, Λ_v and Λ_w, respectively. For neutral stratifications we find Λ_w/z to have a value of about 1. Kaimal (1973) calculated the integral length scale differently but the results should be comparable. More measurements under different meteorological conditions (katabatic flows, SBL with low-level wind maximum, etc.) are needed to resolve this issue in more detail. For instance, Van der Avoird and Duynkerke (1999) and Smedman et al. (1995) show that in more complicated stable

boundary layers the ϕ_m and ϕ_h functions are no longer a linear function of z/Λ, but that they tend to flatten off beyond a certain z/Λ value. This issue might be further resolved by considering the integral length scale as the relevant intrinsic length scale for the parametrization of the turbulence in these type of stable boundary layers.

4. ENERGY BALANCE

The incoming and outgoing shortwave and longwave radiation were measured continuously during May 1998. From the short wave radiation components the albedo was estimated to be about 0.82. As a result of the high albedo the net incoming shortwave radiation (F_S) over the whole month is only about 50 W m^{-2} (see Table 2). The average net-incoming longwave radiation (F_L) is about -37 W m^{-2}. Neither the upward sensible heat flux (H) nor the latent heat flux (LE) is continuously available. However, if we calculate the average of all available hours we obtain 1.8 and 2.4 W m^{-2} for H and LE, respectively. The surface energy balance (Untersteiner, 1961; Herman, 1986) can be summarized as:

$$F_S + F_L = H + LE + I\,, \qquad (4.1)$$

where I is the energy flux into the snow and ice surface. The energy flux into the surface can be due to (short wave) radiation and/or thermal conduction. The upper 15 cm consisted of compact snow for which we use a density ρ_s = 450 kg m^{-3} and a specific heat capacity c_{ps} =

2090 J kg^{-1} K^{-1}. Below 15 cm depth the surface consisted of ice for which we used a density ρ_i = 910 kg m^{-3}, a thermal conductivity λ_i = 2.5 W m^{-1} K^{-1} and a specific heat capacity c_{pi} = 2100 J kg^{-1} K^{-1}. The energy flux I was estimated from temperatures measured at a depth of 5, 10, 20, 30 and 40 cm in the snow and ice. We can integrate the heat storage with time and if we estimate the energy flux through the bottom of the layer zero (z = -0.35 m) from thermal conduction ($\lambda_i \partial T/\partial z$), I can be calculated from:

$$I = \lambda_i \left(\frac{\partial T}{\partial z}\right)_{z = -0.35} + \frac{\partial}{\partial t}\int_{-0.35}^{0} \rho_l \, c_{pl} \, T \, dz \qquad (4.2)$$

where ρ_l and c_{pl} stand for the density of snow (s) or ice (i) as a function of depth. The energy flux through the bottom of the layer (z = -0.35 m), averaged over the whole month of May, is about 0.3 W/m^2, whereas the average value for I, for the whole month of May, is 2.6 W m^{-2}. In summary the net gain by radiation is 12.1 W m^{-2} and the net loss due to sensible and latent heat flux and the energy flux into the surface is 6.8 W m^{-2}. Due to measurement uncertainties there is thus an average imbalance in the surface energy balance ($F_S + F_L - H - LE - I$) of 5.3 W m^{-2} over the whole month of May. Of course positive and negative values in the imbalance partially tend to cancel each other out, which leads to this rather small value. Therefore, it is more realistic to calculate the average of the *absolute* value of the hourly-averaged imbalance ($|F_S + F_L - H - LE - I|$) over the whole month of May; this gives a value of about 15 W/m^2.

Because the radiation instruments have an error of at least 1% in the individual components most of the 15 W/m^2 is probably due to the uncertainty in the measurements made by radiation instruments.

From the study of Untersteiner (1961) and the energy balance presented in Table 2 one might conclude that all energy fluxes are small. This is however not the case if one considers the hourly-averaged energy fluxes. For the period of 1 to 7 May 1998 (Julian Day 121 to 127) we have all the energy fluxes at the ice surface, given by equation (4.1), shown in Figure 8. The net longwave radiation is indicative for the low-cloud cover, small negative values (Figure 8a) indicating that low-clouds are present. For cloud-free situations the net shortwave radiation peaks at solar noon (about 2300 UTC) with values of about 130 $W\ m^{-2}$. The absolute values of the latent heat flux are typically much smaller than those of the sensible heat flux (Figure 8b). Moreover, the latent heat flux is typically positive indicating evaporation from the snow. The sensible heat flux changes from positive to negative for small and large solar zenith angles respectively. There is thus a strong correlation between the sensible heat flux and net shortwave radiation at the surface. The shortwave radiative forcing induces a strong diurnal variation in the snow and ice temperatures with a typical temperature amplitude of about 2 K at a depth of 5 cm below the surface. The ice temperature at 40 cm depth is hardly influenced by the diurnal variation of the energy balance at the surface and shows only a slow change on the time scale of several days. The energy flux into the surface I also shows a strong diurnal variation.

It can thus be concluded that the turbulent fluxes contribute significantly to the hourly-averaged surface energy budget but in the monthly-averaged budget these are small. The high surface albedo of the ice probably gives that the hourly-averaged net-radiation can be large whereas the monthly-averaged values are small. The turbulent fluxes typically follow the "forcing" of the net radiation. On land, having a smaller surface albedo, these findings will be different.

5. FOG AT THE SURFACE

Herman (1986) reviewed the effect of clouds on the Arctic surface energy balance. For May he gives monthly-averaged values for the net longwave and shortwave radiation of –36 and 52 W m^{-2}, respectively. These values are very close to our values given in Table 2. Herman (1986) also showed that the monthly-averaged net radiation at the surface is positive (16 W m^{-2}) and as a consequence heating the ice. Whereas, during cloud-free conditions the net radiation is negative (-7 W m^{-2}) and thus cooling the ice. Therefore it is interesting to study the effect of low clouds on the surface energy balance.

Also during May 1998 clouds were on several occasions present all the way down to the surface. With a Gerber PVM-100A we continuously measured the liquid water content (LWC) and effective radius (r_e) at 2.16m above the surface with a frequency of 1 Hz. An example of a case in which the fog extended down to the surface is shown in Figure 9a. The

time series of LWC show maximum values of about 0.1 g m^{-3} and the effective radius (not shown) is on average about 6 μm. The net longwave radiation increases from its clear sky value (about -75 W m^{-2}) to near zero due to the presence of a cloud several hundred meters thick (Beesley et al., 2000; Bretherton et al., 2000). At the same time all other components of the surface energy balance (4.1) become very small. As an example the energy flux into the surface I is also shown in Figure 9a. The snow temperature (Figure 9b) at 5 cm depth shows a clear diurnal cycle with a maximum value around (solar) noon and a minimum value for the lowest solar zenith angles. When low clouds are present the longwave radiative cooling of the surface is significantly reduced (Figure 9a) and the temperature of the snow does not drop as low as during cloud-free conditions. It is concluded that it is important to have an accurate sea-ice model in order to get the correct diurnal variation in the surface energy balance (Beesley et al., 2000; Bretherton et al., 2000).

6. CONCLUSIONS

We have analyzed turbulence variables in the surface layer of the stable boundary layer. The data were collected at the SHEBA ice camp and above a grass surface at Cabauw, the Netherlands. The turbulent fluxes and variances were measured with a sonic anemometer and a Lyman-Alpha hygrometer with a frequency of 20 Hz. To examine the energy balance of the surface measurements of the net longwave and shortwave radiative fluxes, we also analyzed the temperatures in the upper 40 cm of the ice sheet.

First of all, we computed ogives in order to determine the influence of a cut-off filter length scale on the magnitude of various variances and fluxes. The ogive, Og(f), is the integral of co-spectra between a frequency f and the Nyquist frequency. Ogives are very suitable tools for this kind of analysis, since the graphical representation of ogives clearly shows to what extent the large (meso-)scales contribute to the variance and fluxes. In an ideal situation one would expect to find the minimum spectral energy within a frequency range near the spectral gap that is supposed to separate the small-scale turbulent fluctuations from the larger meso-scale motions. If the frequency f is in the spectral gap range, the ogive of the co-spectrum would acquire a constant value. The examples of variances that were presented here indicated that no distinct spectral gap behavior was exhibited, apart from the vertical velocity variance. The latter finding is rather fortunate since it provides us with an objective way of defining a cut-off filter length scale. The reason is that the vertical velocity variance receives only a marginal contribution from the larger scales, then the same is true for the correlation between the vertical velocity and any other variable, i.e. the vertical flux of this variable. On the basis of the experimental data we used a filter frequency f = 0.01 Hz.

In the parametrization of the stable boundary layer in the ECMWF model the momentum, heat and moisture fluxes are calculated from a turbulent exchange coefficient and from the vertical gradients of wind, potential temperature and moisture. The turbulence exchange coefficient includes a stability function which is based on the gradient Richardson number. From the comparison of the observations with the parametrizations it is concluded that the

ECMWF model will predict fluxes which are too large (absolute value) compared with the observed values. This is agreement with earlier findings (Beljaars and Viterbo, 1998), namely that the stable boundary layer in the ECMWF model tends to be too deep over flat terrain.

Further, we investigated the behavior of the integral length scale (Λ_w) for the vertical velocity as a function of stability. The integral length scale represents the size of the energetically most dominant eddies and therefore could be a natural candidate to serve as a characteristic turbulence length scale. Our choice of the integral length scale as a master length scale is motivated by the fact that for stable boundary layers the flux-profile relationships include a dependency on z (the height above the surface). Nevertheless, it is widely recognized that, particularly at large heights in the SBL, local turbulence conditions are completely decoupled from the direct influence of the surface (Nieuwstadt, 1984). We found that by substituting Λ_w for the height z, the flux-profile relationship ϕ'_m,

$$\phi'_m = \frac{\kappa \Lambda_w}{u_*} \frac{\partial \bar{u}}{\partial z}$$

becomes almost independent of stability z/Λ. This promising result should however be verified for a wider range of conditions, such as katabatic flows or stable boundary layers

with a low-level jet. We therefore recommended that more measurements be performed under such conditions.

The surface energy balance of the Arctic sea ice during May 1998 was dominated mainly by radiative fluxes. The presence of clouds had a significant impact on the distribution of the radiation. For example, when low stratus was present the net upward longwave radiation approached a value near zero, which is in contrast with its clear sky value of about -75 W/m^2. The monthly-averaged net loss due to sensible and latent heat fluxes from the snow was rather small (4.2 W/m^2). At first sight, this seems to suggest that turbulence plays only a minor role in the surface energy balance. However, detailed inspection of the diurnal variations of the turbulent fluxes indicated that although their time-averaged values were small, their instantaneous values were not. The observed stable boundary layers above the sea ice discussed in this paper could be characterized as weakly stable (Mahrt, 1998), since typically $z/\Lambda < 0.6$. The formation of very stable boundary layers was prevented in this case since the temperatures remained relatively close to those of the adjacent air above, as was illustrated by the distinct diurnal cycle of the sea ice temperatures.

Acknowledgement

The last author's participation in the SHEBA experiment was supported by the Netherlands Geosciences Foundation (GOA) with financial aid (GRANT 750.295.03A) from the Netherlands Organization for Scientific Research (NWO). The IMAU wishes to thank the

many people of the FIRE/SHEBA community who gave logistical support by bringing the equipment to the SHEBA ice camp and who also assisted on site.

6. REFERENCES

Andreas, E.L., Spectral measurements in a disturbed boundary layer over snow. J. Atmos. Sci., 44, 1912-1939, 1987.

Beesley, J.A., C.S. Bretherton, C. Jakob, E.L. Andreas, J.M. Intrieri and T.A. Uttal, A comparison of cloud and boundary-layer variables in the ECMWF forecast model with observations at Surface Heat Budget of the Arctic Ocean (SHEBA) ice camp. J. Geophys. Res., 105, 12337-12349, 2000.

Beljaars, A.C.M. and P. Viterbo, Role of the boundary layer in a numerical weather prediction model, 287-304. In: Holtslag A.A.M. and P.G. Duynkerke (editors), 1998: Clear and Cloudy Boundary Layers. Royal Netherlands Academy of Sciences, PO Box, 19121, 1000 GC Amsterdam, The Netherlands, 372pp, 1998.

Bretherton, C. S., S. R. de Roode, C. Jakob, E. A. Andreas, J. Intrieri, R. E. Moritz, and P. O. G. Persson, 2000: A comparison of the ECMWF forecast model with observations over the annual cycle at SHEBA. (revised version submitted to J. Geophys. Res.), 2000.

Brost, R. A., and J. C. Wyngaard, A model study of the stably stratified planetary boundary layer. J. Atmos. Sci., 35, 1427-1440, 1978.

Campbell Scientific, CSAT3 three-dimensional sonic anemometer instruction manual. 13pp. Obtainable from: Campbell Scientific Inc., 815 West 1800 North, Logan, Utah 84321-1784, USA, 1996.

Caughey, S. J., J. C. Wyngaard and J. C. Kaimal, Turbulence in the evolving stable boundary layer. J. Atmos. Sci., 6, 1041-1052, 1979.

Davis, A., A. Marshak, W. Wiscombe and R.F. Cahalan, Scale invariance of liquid water distribution in marine stratocumulus. Part I: spectral properties and stationarity issues. J. Atmos. Sci., 53, 1538-1558, 1996.

Derbyshire, S.H., Nieuwstadt's stable boundary layer revisited. Quart. J. Roy. Meteorol. Soc., 116, 127-158, 1990.

Duynkerke, P.G., Turbulence, radiation and fog in Dutch stable boundary layers. Boundary-Layer Meteorol., 90, 447-477, 1999.

Garratt, J. R., The atmospheric boundary layer. Cambridge University Press, 316 pp, 1992.

Herman, G. F., Arctic stratus clouds. In the geophysics of sea ice, N. Untersteiner (Ed.), 465-488, Plenum Press, New York, 1986.

Högström, U., Non-dimensional wind and temperature profiles in the atmospheric surface layer: a re-evaluation. Boundary-Layer Meteorol., 42, 55-78, 1988.

Högström, U., Review of some basic characteristics of the atmospheric surface layer. Boundary-Layer Meteorol., 78, 215-246, 1996.

Kaimal, J. C., Turbulence spectra, length scales and structure parameters in the stable surface layer. Boundary-Layer Meteorol., 4, 289-309, 1973.

King, J. C., Some measurements of turbulence over an Antarctic ice shelf. Quart. J. Roy. Meteorol. Soc., 166, 379-400, 1990.

Larsson, L., Measurements and modeling of turbulence characteristics in stable boundary layers. IMAU Report, V97-25, Obtainable from: IMAU, Utrecht University, Princetonplein 5, 3584 CC Utrecht, The Netherlands, 1997.

Mahrt, L., Surface fluxes and boundary layer structure. 113-128. In: Holtslag A.A.M. and P.G. Duynkerke (editors), 1998: Clear and Cloudy Boundary Layers. Royal Netherlands Academy of Sciences, PO Box, 19121, 1000 GC Amsterdam, The Netherlands, 372pp, 1998.

Mahrt, L., R. C. Heald, D. H. Lenschow, and B. B. Stankov, An observational study of the structure of the nocturnal boundary layer. Boundary-Layer Meteorol., 17, 247-264, 1979.

Mierij Meteo, Lyman-α hygrometer. User Manual, 14pp. Obtainable from: Mierij Meteo BV, Weltevreden 4c, 3731 AL De Bilt, The Netherlands, 1997.

Monna, W.A.A., and J.G. van der Vliet, Facilities for research and weather observations on the 213 m tower at Cabauw and at remote locations. Sci. Rep. WR 87-5. Obtainable from: KNMI, PO Box 201, 3730 AE, De Bilt, The Netherlands, 1987.

Nieuwstadt, F.T.M., The turbulent structure of the stable, nocturnal boundary layer. J. Atmos. Sci., 41, 2202-2216, 1984.

Oncley, S.P., C.A. Friehe, J.C. Larue, J.A. Businger, E.C. Itsweire, and S.S. Chang, Surface-layer fluxes, profiles, and turbulence measurements over uniform terrain under near-neutral conditions. J. Atmos. Sci., 53, 1029-1044, 1996.

Pinto, J.O., J.A. Curry, A.H. Lynch and P.O.G. Persson, Modeling clouds and radiation for the November 1997 period of SHEBA using a column climate model. J. Geophys. Res., 104, 6661-6678, 1999.

Roode, S.R. de, W. Boot, P.G. Duynkerke and J.C.H. Van der Hage, Surface and tethered-balloon observations of actinic flux: effects of Arctic stratus, surface albedo and solar zenith angle. (submitted to J. Geophys. Res. D), 2000.

Stull, R. B., An introduction to boundary-layer meteorology. Kluwer Academic Publishers, 666 pp, 1988.

Smedman, A.-S., Bergström, H. and Högström, U., Spectra, variances and length scales in a marine stable boundary layer dominated by a low level jet. Boundary-Layer Meteorol., 76, 211-232, 1995.

Untersteiner, N., On the mass and heat budget of arctic sea ice. Arch. Met. Geophys. Bioklim. A, 12, 151-182, 1961.

Van der Avoird, E. and P.G. Duynkerke, Turbulence in a katabatic flow: Does it resemble turbulence in stable boundary layers over flat surfaces? Boundary-Layer Meteorol., 92, 39-66, 1999.

Van Ulden, A.P and J. Wieringa, Atmospheric boundary layer research at Cabauw. Boundary-Layer Meteorol., 78, 39- 69, 1996.

Wyngaard, J. C., Modeling the planetary boundary-layer. Extension to the stable case. Boundary-Layer Meteorol., 9, 441-460, 1975.

Yamada, T., PBL similarity profiles determined from a level-2 turbulence closure model. Boundary-Layer Meteorol., 17, 333-351, 1979.

Table Captions

Table 1. The standard deviation of the velocity fluctuations normalized with the friction velocity u_* for May 1998 at the SHEBA site, both for the filtered and unfiltered data.

Table 2. The components of the surface energy balance (4.1) averaged over the month of May 1998 at the SHEBA site.

	σ_u/u_*	σ_v/u_*	σ_w/u_*
filtered	2.31±0.15	1.92±0.15	1.35±0.11
unfiltered	2.96±0.52	2.63±0.62	1.26±0.13

Table 1. The standard deviation of the velocity fluctuations normalized with the friction velocity u_* for May 1998 at the SHEBA site, both for the filtered and unfiltered data.

	F_S	F_L	H	LE	I
W m^{-2}	49.9	-37.8	1.8	2.4	2.6

Table 2. The components of the surface energy balance (4.1) averaged over the month of May 1998 at the SHEBA site.

Figure Captions

Figure 1. Ogives of a) velocity variances (for $\overline{u'u'}$, $\overline{v'v'}$ and $\overline{w'w'}$) and b) vertical momentum fluxes ($\overline{u'w'}$ and $\overline{v'w'}$) as a function of frequency for 1100 to 1200 UTC 1 May 1998. For the hour considered $\bar{u}$ = 6. 8 m/s and $z/\Lambda = 0.001$.

Figure 2. Ogives of a) temperature and humidity variances ($\overline{T'T'}$ and $\overline{q'q'}$) and b) vertical heat and moisture fluxes ($\overline{w'T'}$ and $\overline{w'q'}$) as a function of frequency for 1100 to 1200 UTC 1 May 1998.

Figure 3. The normalized standard deviation of the vertical velocity fluctuations as a function of stability z/Λ: FIRE III • and Cabauw ◦.

Figure 4. a) The non-dimensional wind gradient ϕ_m as a function of stability z/Λ: FIRE III •, Cabauw ◦ and $\phi_m = 1 + 4\, z/\Lambda$ (solid line). The stability correction for momentum f_m b) and heat f_h c) in the turbulent exchange coefficient (3.6) as a function of the gradient Richardson number Ri_g: Cabauw ◦, $\phi_m = \phi_h = 1 + 4\, z/\Lambda$ (solid line) and ECMWF surface layer (long-dash) and stable boundary layer (short-dash) formulation.

Figure 5. For the vertical velocity the autocorrelation function $\rho_w(\xi)$ (solid line) and its integral (dashed line) as a function of the space lag ξ for 1000 to 1100 UTC 1 May 1998: a) linear horizontal axis and b) logarithmic horizontal axis.

Figure 6. The integral length scale of the vertical velocity Λ_w normalized with the measurement height z as a function of stability z/Λ: FIRE III •, Cabauw ◦ and equation (3.10) ($(1 + 4\ z/\Lambda)^{-1}$; solid line).

Figure 7. The non-dimensional wind gradient ϕ'_m as a function of stability z/Λ: FIRE III • and Cabauw ◦.

Figure 8. For the period 1 to 7 May 1998 (Julian Day 121 to 127) the time variation of the components of the surface energy balance: a) net downward shortwave radiation (F_S) and net downward longwave radiation (F_L), b) sensible heat flux (H), latent heat flux (LE) and net energy flux into the surface (I) and c) snow and ice temperatures at a depth of 0.05, 0.1, 0.2, 0.3 and 0.4 m.

Figure 9. For the period 20 to 22 May 1998 (Julian Day 140 to 142) the time variation of the: net downward long wave radiation (F_L), net energy flux into the surface (I) and liquid water content (LWC) and b) snow and ice temperatures at a depth of 0.05, 0.1, 0.2, 0.3 and 0.4 m.

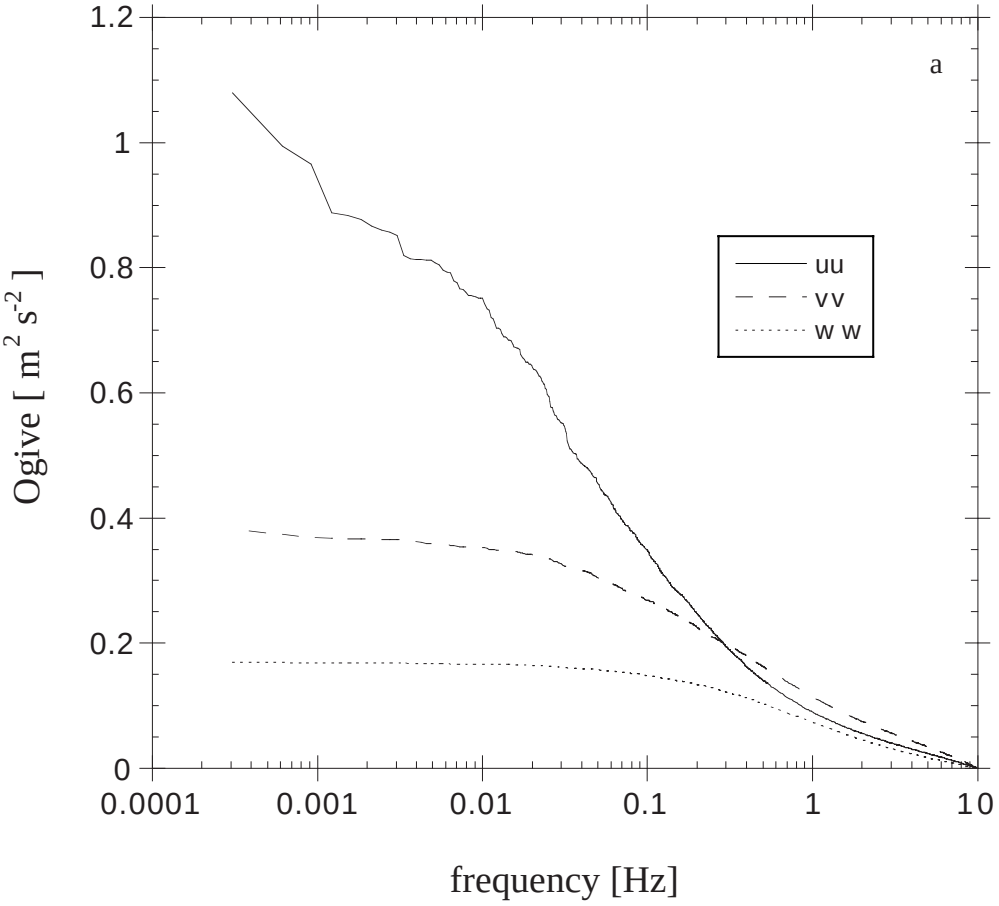

Figure 1. Ogives of a) velocity variances (for $\overline{u'u'}$, $\overline{v'v'}$ and $\overline{w'w'}$) and b) vertical momentum fluxes ($\overline{u'w'}$ and $\overline{v'w'}$) as a function of frequency for 1100 to 1200 UTC 1 May 1998. For the hour considered $\bar{u}$ = 6. 8 m/s and z/Λ = 0.001.

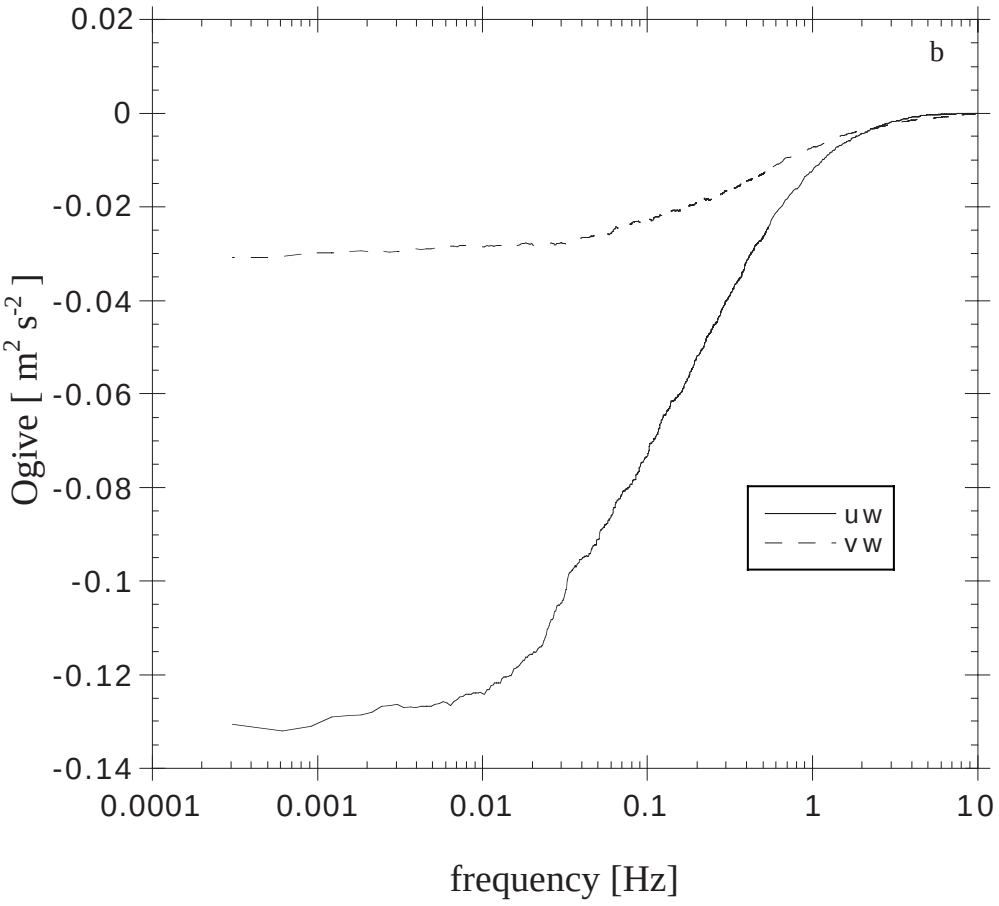

Figure 1. Ogives of a) velocity variances (for $\overline{u'u'}$, $\overline{v'v'}$ and $\overline{w'w'}$) and b) vertical momentum fluxes ($\overline{u'w'}$ and $\overline{v'w'}$) as a function of frequency for 1100 to 1200 UTC 1 May 1998. For the hour considered $\bar{u}$ = 6. 8 m/s and $z/\Lambda = 0.001$.

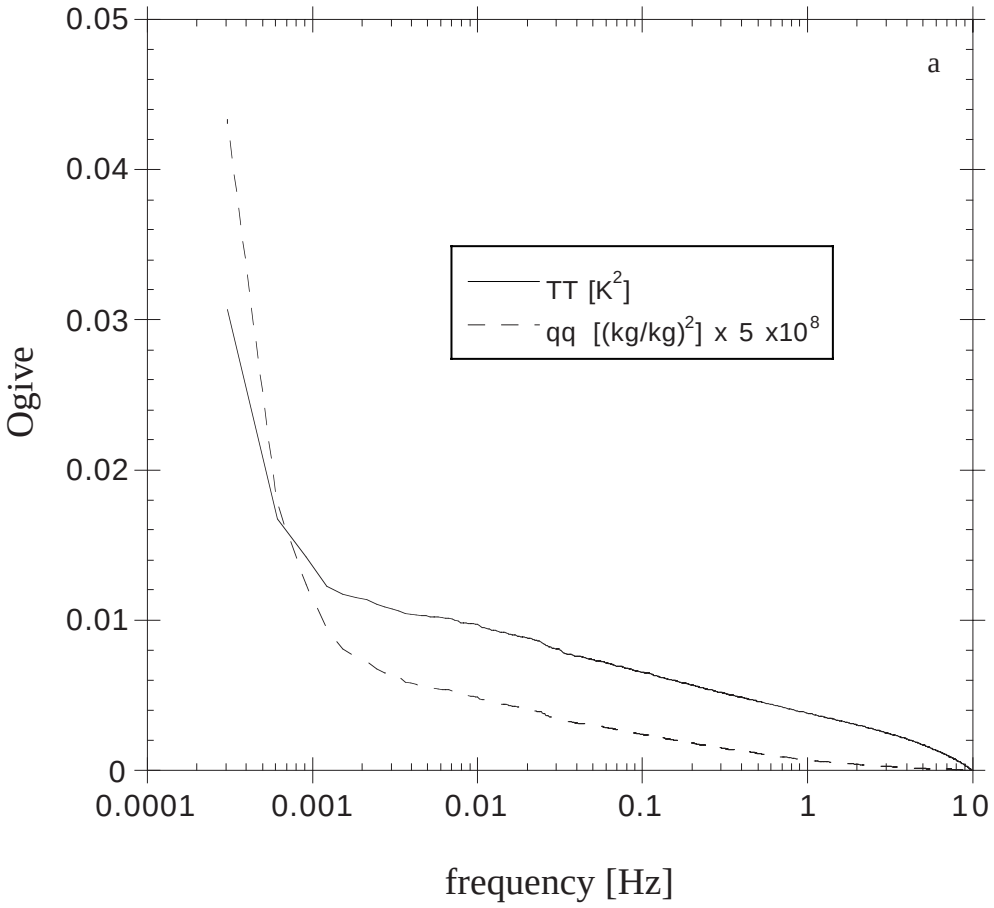

Figure 2. Ogives of a) temperature and humidity variances ($\overline{T'T'}$ and $\overline{q'q'}$) and b) vertical heat and moisture fluxes ($\overline{w'T'}$ and $\overline{w'q'}$) as a function of frequency for 1100 to 1200 UTC 1 May 1998.

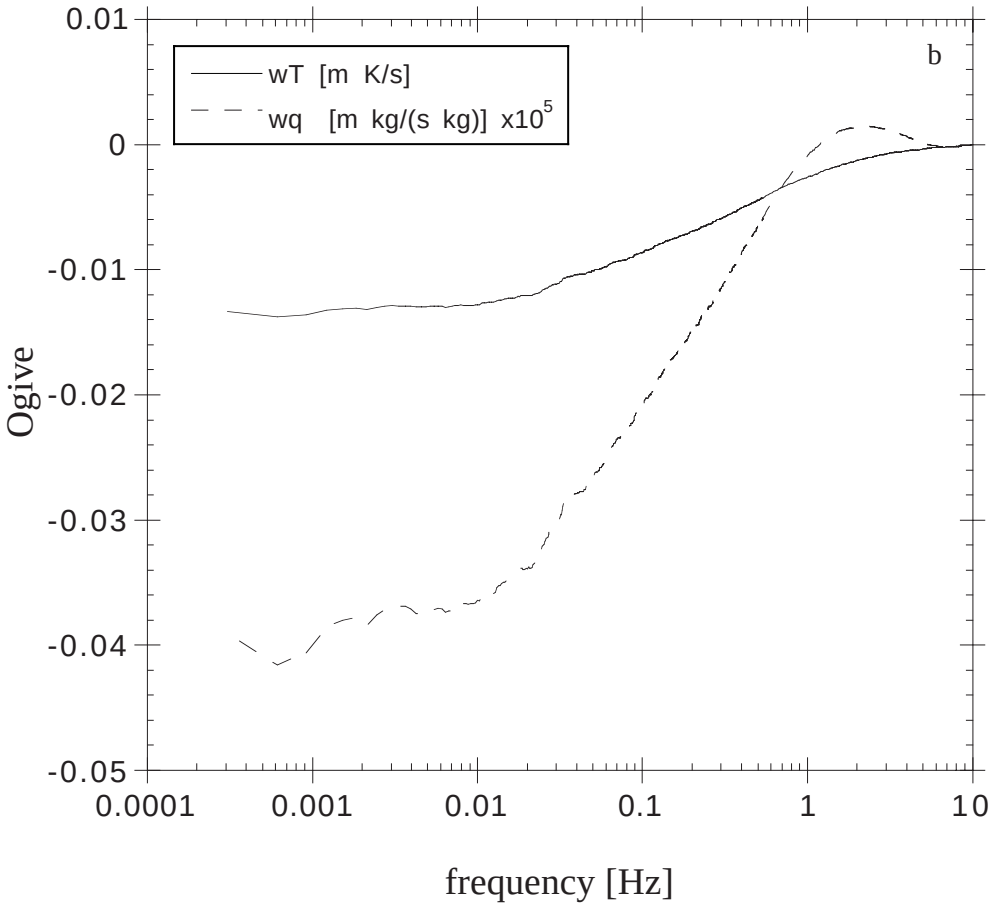

Figure 2. Ogives of a) temperature and humidity variances ($\overline{T'T'}$ and $\overline{q'q'}$) and b) vertical heat and moisture fluxes ($\overline{w'T'}$ and $\overline{w'q'}$) as a function of frequency for 1100 to 1200 UTC 1 May 1998.

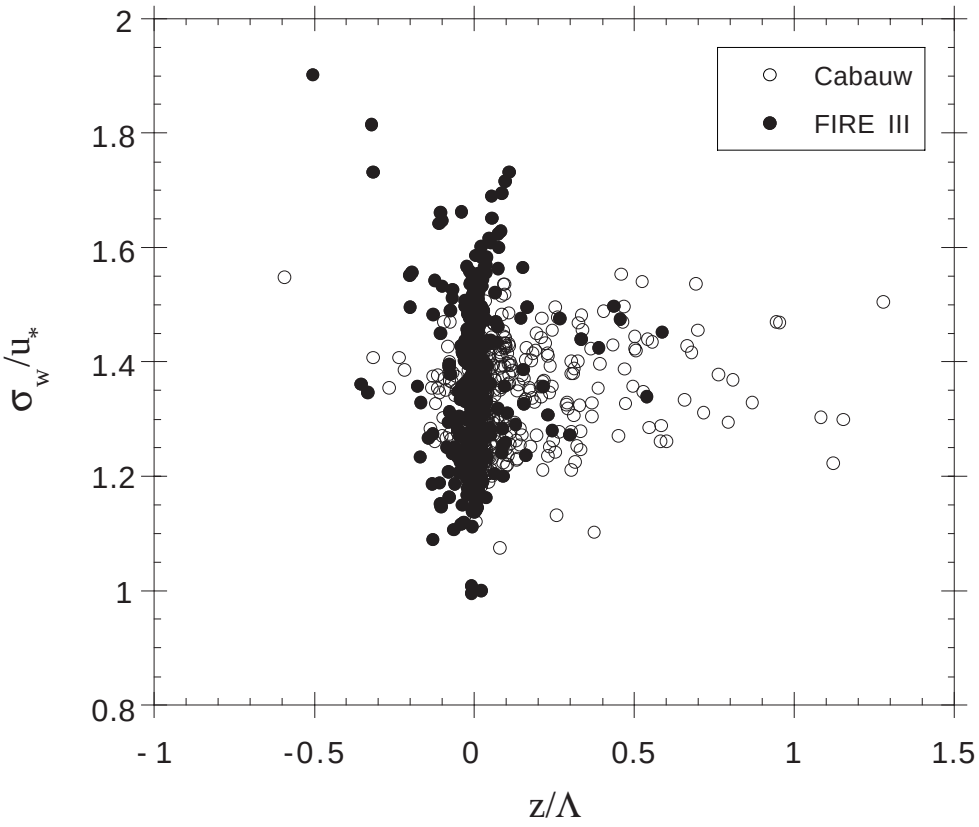

Figure 3. The normalized standard deviation of the vertical velocity fluctuations as a function of stability z/Λ: FIRE III • and Cabauw ◦.

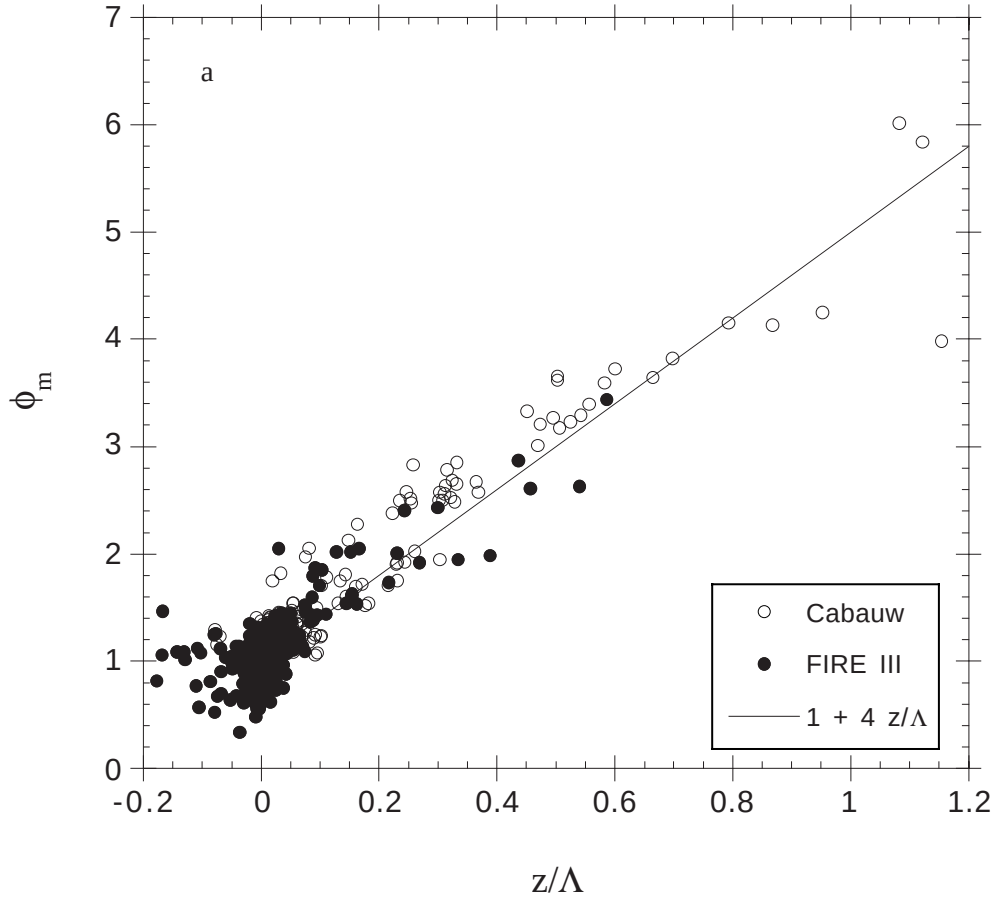

Figure 4. a) The non-dimensional wind gradient ϕ_m as a function of stability z/Λ: FIRE III •, Cabauw ◦ and $\phi_m = 1 + 4\ z/\Lambda$ (solid line). The stability correction for momentum f_m b) and heat f_h c) in the turbulent exchange coefficient (3.6) as a function of the gradient Richardson number Ri_g: Cabauw ◦, $\phi_m = \phi_h = 1 + 4\ z/\Lambda$ (solid line) and ECMWF surface layer (long-dash) and stable boundary layer (short-dash) formulation.

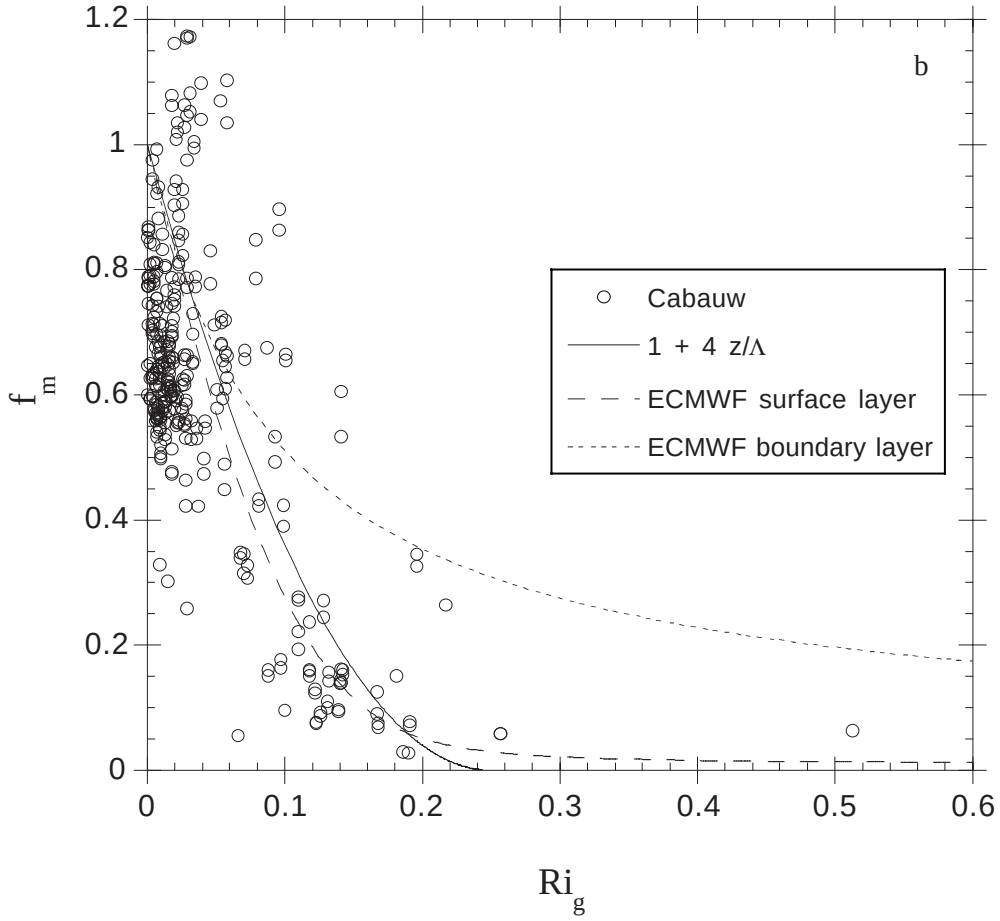

Figure 4. a) The non-dimensional wind gradient ϕ_m as a function of stability z/Λ: FIRE III •, Cabauw ◦ and $\phi_m = 1 + 4\ z/\Lambda$ (solid line). The stability correction for momentum f_m b) and heat f_h c) in the turbulent exchange coefficient (3.6) as a function of the gradient Richardson number Ri_g: Cabauw ◦, $\phi_m = \phi_h = 1 + 4\ z/\Lambda$ (solid line) and ECMWF surface layer (long-dash) and stable boundary layer (short-dash) formulation.

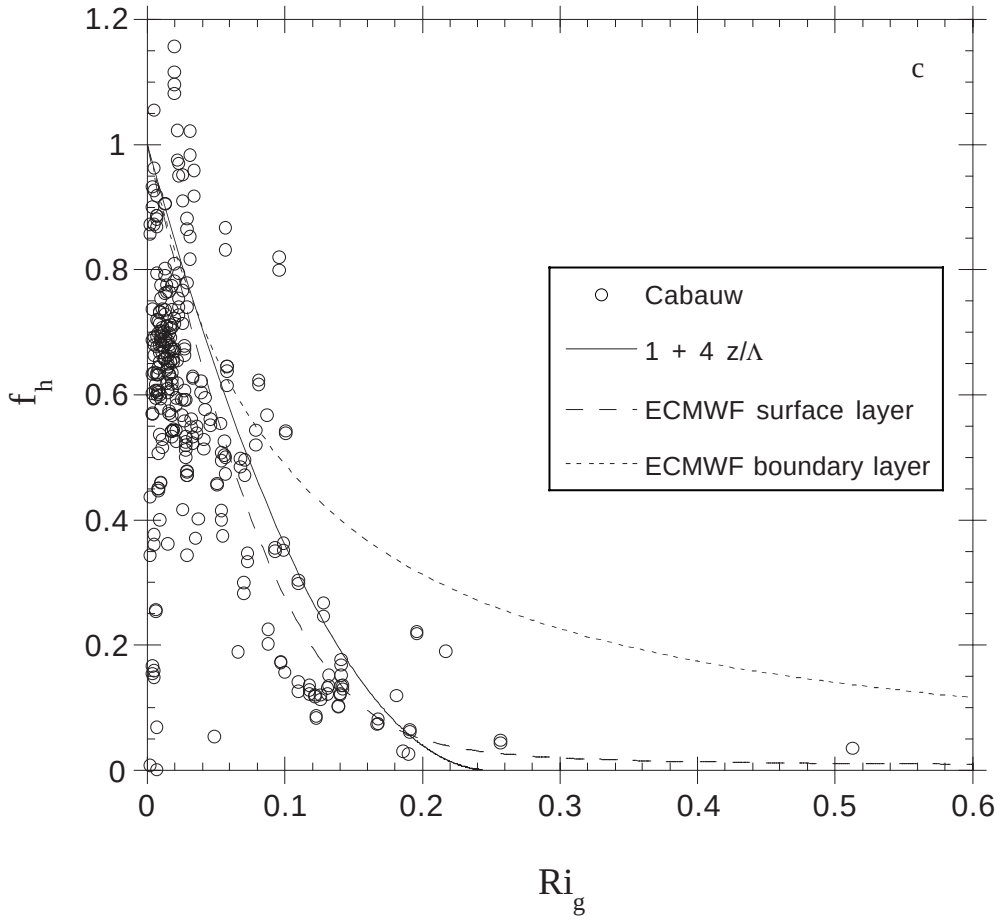

Figure 4. a) The non-dimensional wind gradient ϕ_m as a function of stability z/Λ: FIRE III •, Cabauw ◦ and $\phi_m = 1 + 4\ z/\Lambda$ (solid line). The stability correction for momentum f_m b) and heat f_h c) in the turbulent exchange coefficient (3.6) as a function of the gradient Richardson number Ri_g: Cabauw ◦, $\phi_m = \phi_h = 1 + 4\ z/\Lambda$ (solid line) and ECMWF surface layer (long-dash) and stable boundary layer (short-dash) formulation.

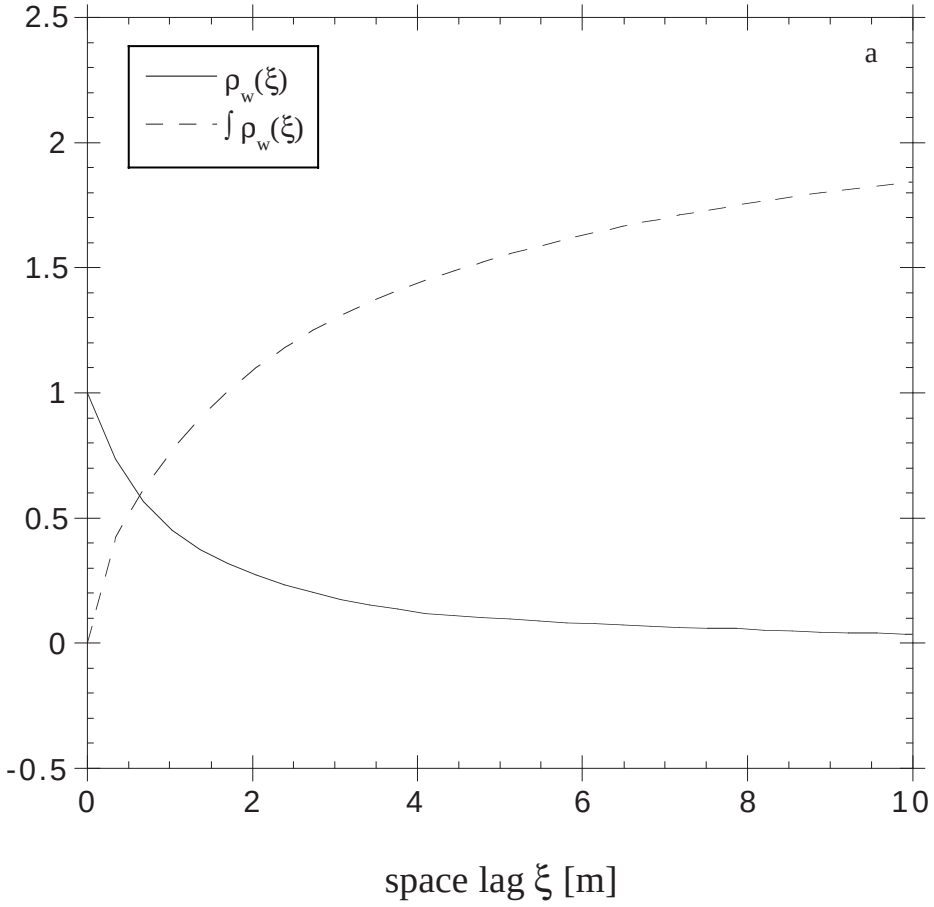

Figure 5. For the vertical velocity the autocorrelation function $\rho_w(\xi)$ (solid line) and its integral (dashed line) as a function of the space lag ξ for 1000 to 1100 UTC 1 May 1998: a) linear horizontal axis and b) logarithmic horizontal axis.

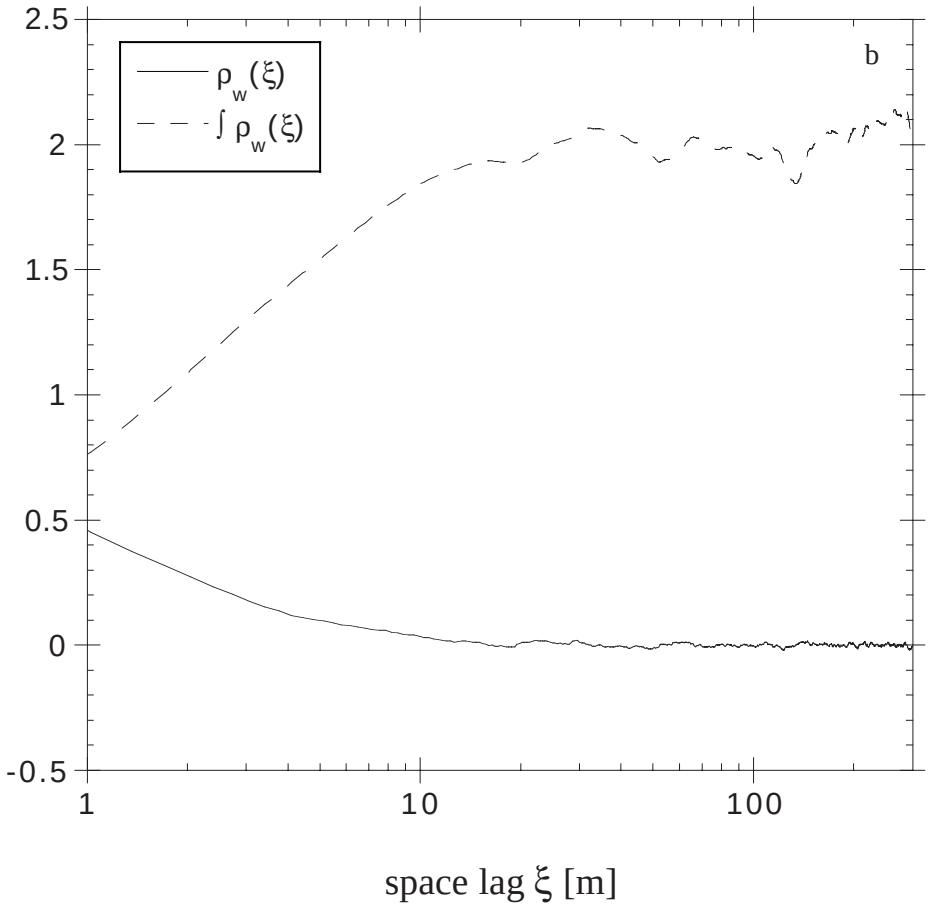

Figure 5. For the vertical velocity the autocorrelation function $\rho_w(\xi)$ (solid line) and its integral (dashed line) as a function of the space lag ξ for 1000 to 1100 UTC 1 May 1998: a) linear horizontal axis and b) logarithmic horizontal axis.

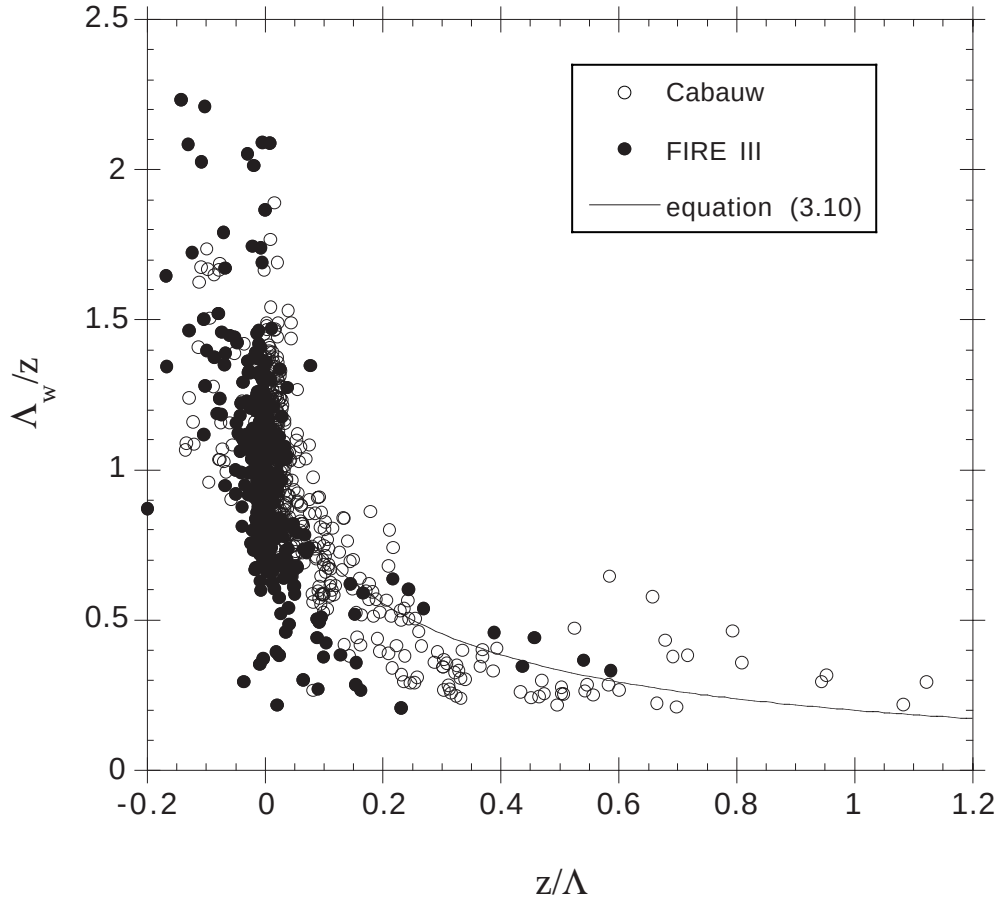

Figure 6. The integral length scale of the vertical velocity Λ_w normalized with the measurement height z as a function of stability z/Λ: FIRE III •, Cabauw ◦ and equation (3.10) ($(1 + 4\ z/\Lambda)^{-1}$; solid line).

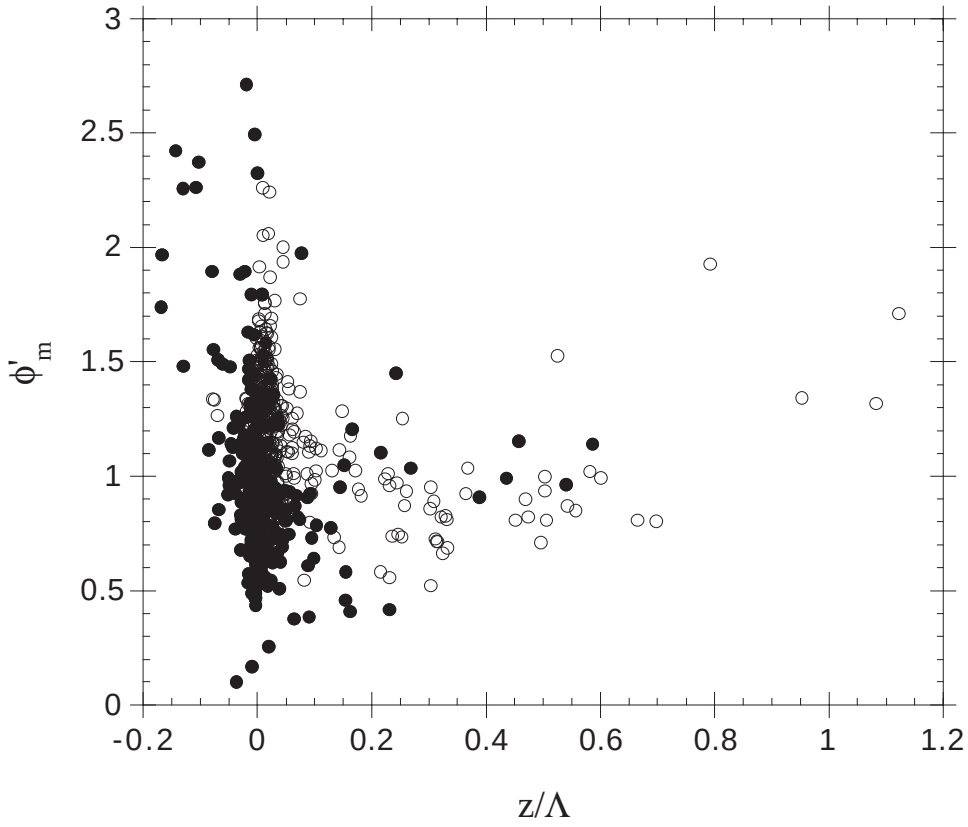

Figure 7. The non-dimensional wind gradient ϕ'_m as a function of stability z/Λ: FIRE III • and Cabauw ◦.

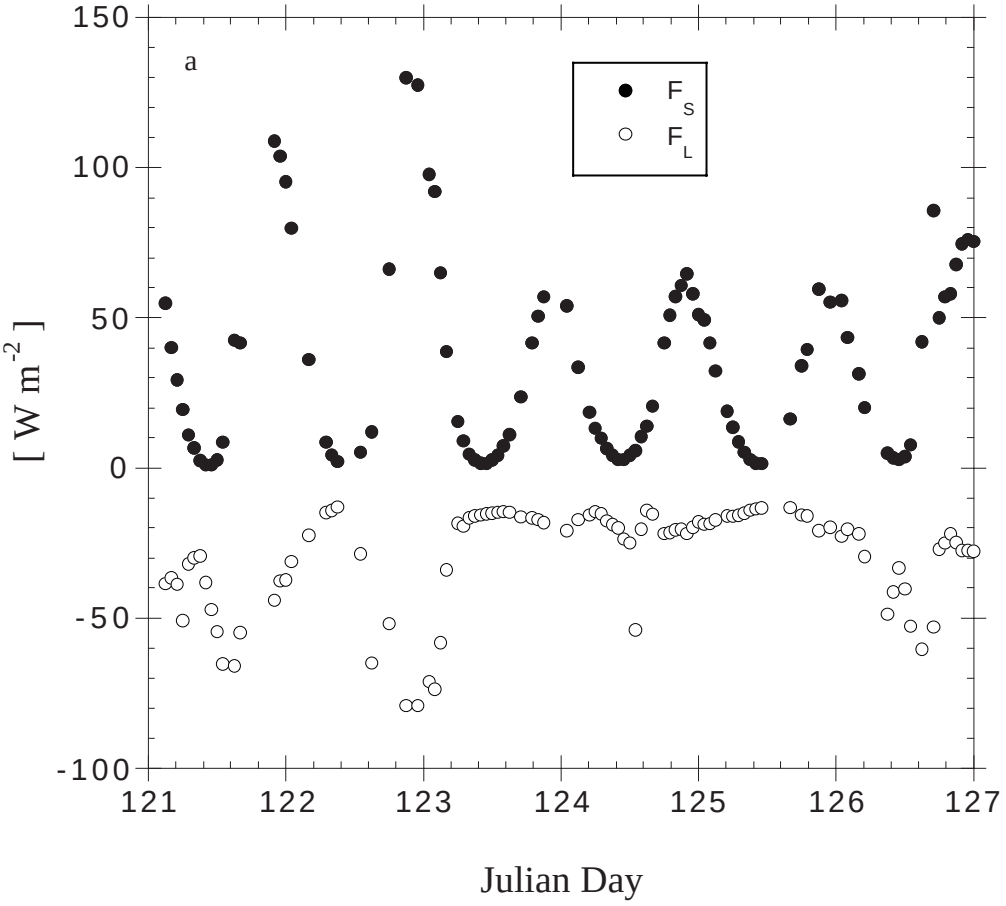

Figure 8. For the period 1 to 7 May 1998 (Julian Day 121 to 127) the time variation of the components of the surface energy balance: a) net downward shortwave radiation (F_S) and net downward longwave radiation (F_L), b) sensible heat flux (H), latent heat flux (LE) and net energy flux into the surface (I) and c) snow and ice temperatures at a depth of 0.05, 0.1, 0.2, 0.3 and 0.4 m.

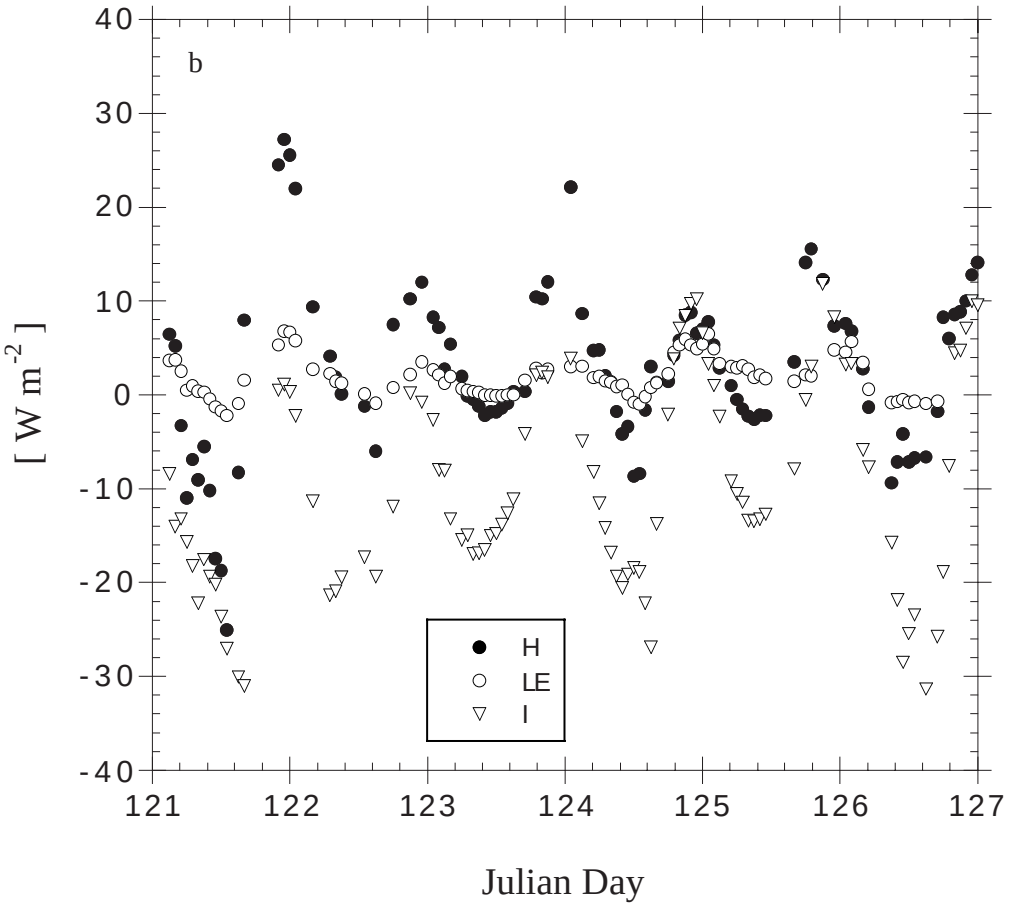

Figure 8. For the period 1 to 7 May 1998 (Julian Day 121 to 127) the time variation of the components of the surface energy balance: a) net downward shortwave radiation (F_S) and net downward longwave radiation (F_L), b) sensible heat flux (H), latent heat flux (LE) and net energy flux into the surface (I) and c) snow and ice temperatures at a depth of 0.05, 0.1, 0.2, 0.3 and 0.4 m.

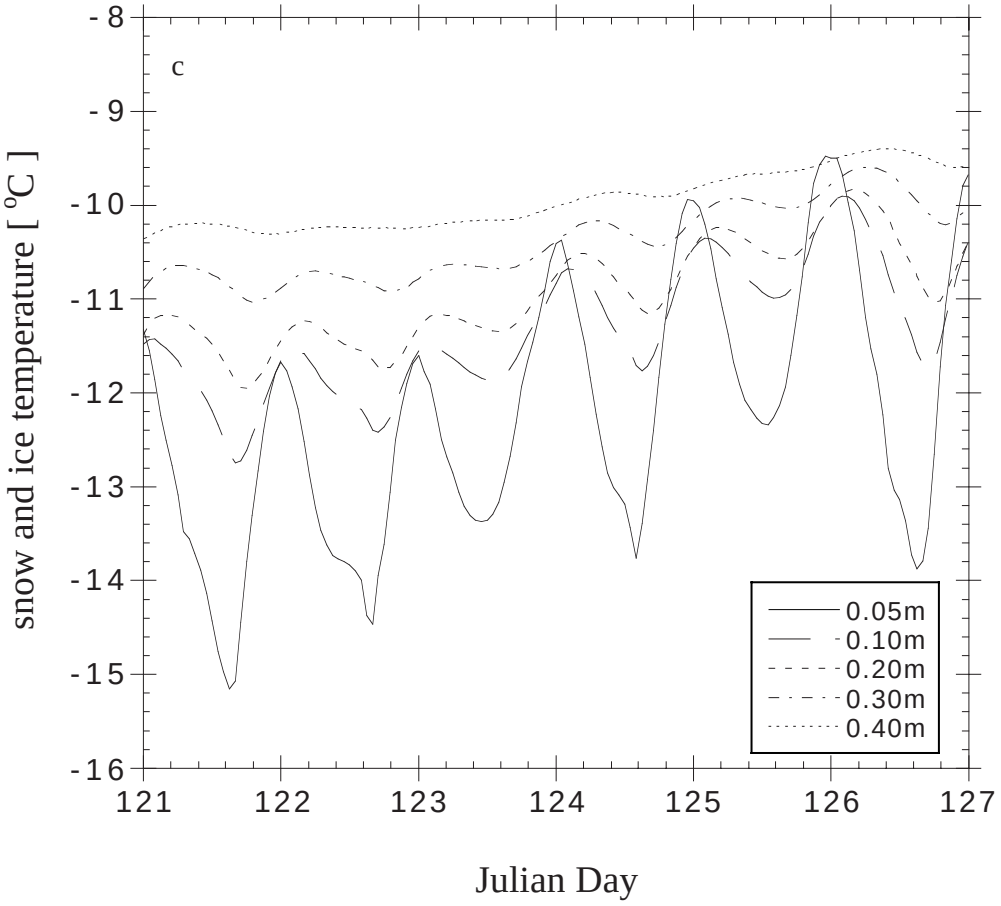

Figure 8. For the period 1 to 7 May 1998 (Julian Day 121 to 127) the time variation of the components of the surface energy balance: a) net downward shortwave radiation (F_S) and net downward longwave radiation (F_L), b) sensible heat flux (H), latent heat flux (LE) and net energy flux into the surface (I) and c) snow and ice temperatures at a depth of 0.05, 0.1, 0.2, 0.3 and 0.4 m.

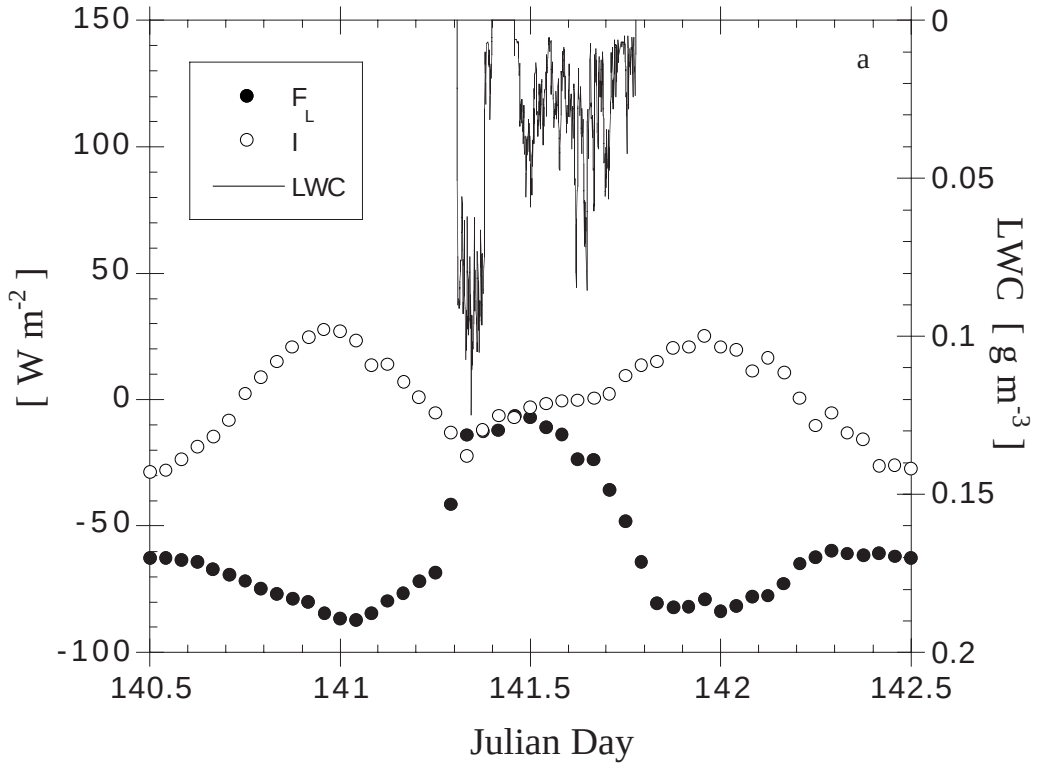

Figure 9. For the period 20 to 22 May 1998 (Julian Day 140 to 142) the time variation of the: net downward long wave radiation (F_L), net energy flux into the surface (I) and liquid water content (LWC) and b) snow and ice temperatures at a depth of 0.05, 0.1, 0.2, 0.3 and 0.4 m.

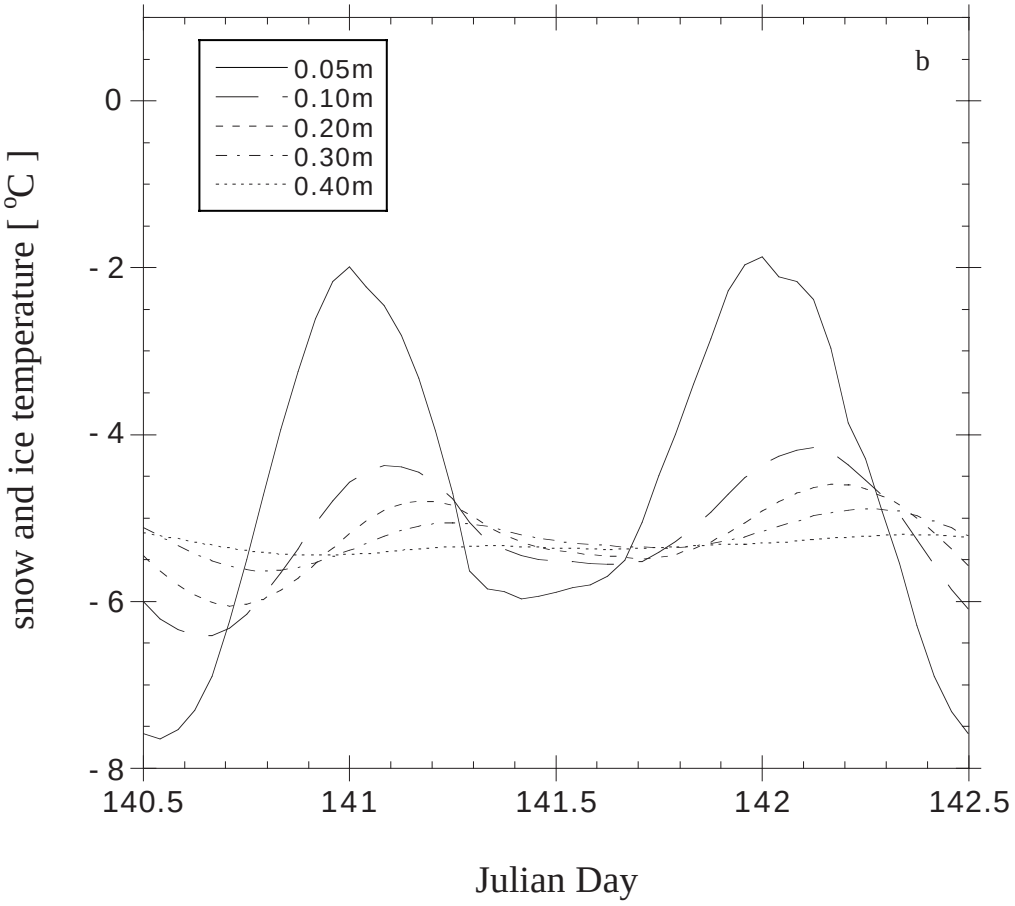

Figure 9. For the period 20 to 22 May 1998 (Julian Day 140 to 142) the time variation of the: net downward long wave radiation (F_L), net energy flux into the surface (I) and liquid water content (LWC) and b) snow and ice temperatures at a depth of 0.05, 0.1, 0.2, 0.3 and 0.4 m.